

# **Breaking two laser “axioms”: Lasing without inversion and thermal equilibrium**

**Rafi Weill, Alexander Bekker, Boris Levit, Michael Zhurahov and Baruch Fischer**

The Andrew & Erna Viterbi Faculty of Electrical Engineering, Technion, Haifa 32000, Israel

E-mail: [fischer@ee.technion.ac.il](mailto:fischer@ee.technion.ac.il)

## **Abstract:**

It is well known that lasing requires population inversion and that lasers are not in thermal equilibrium (TE). There is a singular example for lasing without inversion (LWI) based on a subtle quantum interference effect that was presented and observed many years ago but has not become a spread and practical method<sup>1-6</sup>. Photons were found to be in TE in a special microcavity but not in a lasing regime<sup>7,8</sup>. Here we report on experimental findings that break these two “axioms” on lasers. We show LWI and TE in regular lasers with standard erbium-doped fibers (edf) at the 1550nm wavelength regime. The TE is observed for photons in edf cavities and even in open fibers in broad wavelength ranges up to ~200nm. The thermal-LWI results from photon thermalization that spreads the spectrum and transforms photons from low to high wavelengths where the emission cross section is larger than the absorption and compensates for the lower upper-state population. The experimental results are supported by a theoretical analysis based on the rate equations.

The concept of lasing without inversion (LWI) refers to a situation where quantum interference of atomic transitions eliminates absorption but allows stimulated emission, gain and lasing<sup>1-5</sup>. It was presented and observed many years ago but has not become a spread and practical method. It is related to coherent population trapping (CPT) and electromagnetically induced transparency (EIT)<sup>6</sup>. In this work we experimentally find a new and very different lasing without population inversion phenomenon in standard broadband edf lasers. It is a non-quantum, but thermal lasing without inversion (T-LWI) effect.

The second phenomenon in the present work is thermal equilibrium (TE) in fibers and lasers that is against the common view that lasers are not in TE. These *thermal lasers* are the base for the T-LWI which can also be a platform for Bose-Einstein condensation (BEC). Photon-BEC was firstly demonstrated in a remarkable experimental work with a dye-filled microcavity<sup>7,8</sup>, that followed other papers on BEC with non-atomic bosons, such as polaritons and magnons<sup>9-11</sup>. It also initiated theoretical studies, discussions and questions about the nature of photon-BEC in optical cavities, the relation to lasers<sup>12-15</sup>, and to classical condensation<sup>16-24</sup>. The photon thermalization and BEC experiment was observed not in the lasing regime but much below it, and in addition required strict conditions<sup>7,8</sup>. They included a micron-size cavity with a two-dimensional (2D) confinement of lateral modes, very high mirror reflectivities that provided high finesse to trap the photons in a “white wall photon box”, and very low losses. They also needed a very high capture of the spontaneously emitted photons in all directions and a cutoff frequency. All these requirements were crucial for TE and BEC. The theoretical studies discussed the main differences between a low loss quantum-statistics regime that can yield TE and BEC, and a higher losses regime of classical lasers<sup>12,13,25,26</sup>. In our work we find that for edf systems many of the above restriction are relaxed, and photon TE is obtained in standard one-dimensional (1D) edf cavities, in the lasing regime with T-LWI, and even in open fibers.

Erbium-doped fibers (edf) are widely used as amplifiers in fiber optic communication. Erbium is a “three level” atom system with broad levels due to Stark splittings (Stark manifolds) that can provide gain at the 1550nm wavelength regime, commonly between 1530-1560nm (the C-band)<sup>27</sup>. The pumping from the first to the third level is usually done with wavelengths at  $\sim 980\text{nm}$  or  $\sim 1470\text{ nm}$ . The spontaneous emission time between the two main levels is  $t_{sp} \sim 10\text{ms}$ .

The slightly shifted absorption and emission wavelength dependent cross sections  $\sigma_{12}(\lambda)$  and  $\sigma_{21}(\lambda)$ , which are related to transitions between the first and second levels, are shown in Fig. 1.

These cross sections usually follow the McCumber<sup>27-29</sup> (or Kennard-Stepanov<sup>30,31</sup>) relation<sup>26</sup>  $\sigma_{12}(\nu)/\sigma_{21}(\nu) = B_{12}(\nu)/B_{21}(\nu) \propto e^{\beta h\nu}$ , where  $B_{ij}(\nu)$  are the Einstein coefficients,  $\nu$  and  $\lambda$  are frequency and wavelength,  $\nu\lambda = c/n_r$ ,  $c$  is the speed of light, and  $n_r$  is the refractive index. We note that the usual Einstein relation  $B_{12} = B_{21}$  (and more generally  $g_1 B_{12} = g_2 B_{21}$ , where  $g_i$  is the degeneracy factor) holds for a specific wavelength transition. The temperature dependent asymmetry in  $\sigma_{12}(\nu) \neq \sigma_{21}(\nu)$  results from the sublevels thermal occupation. The broad sublevels of each of these two levels thermalize in a time scale of  $t_a \sim 0.2-0.7\text{ ps}$  due to interaction with the silica host<sup>27</sup>. Without photon-photon interaction the photon thermalization depends on interaction with the erbium atoms. The time scale for such successive photon-erbium scattering is  $t_p$  and the photon lifetime in the cavity is  $t_c$ . In our fiber systems  $t_p \ll t_c$ , as we discuss below, and therefore there are many photon-erbium interaction cycles that are needed for photon thermalization. Another loss factor results from the small fraction  $\kappa$  of the spontaneous emission photons captured in the fiber. The microcavity experiment and the theory required that those photons are overwhelmingly captured in the cavity<sup>7,8,12,13</sup>, but, as we show below, it is not needed in our systems.

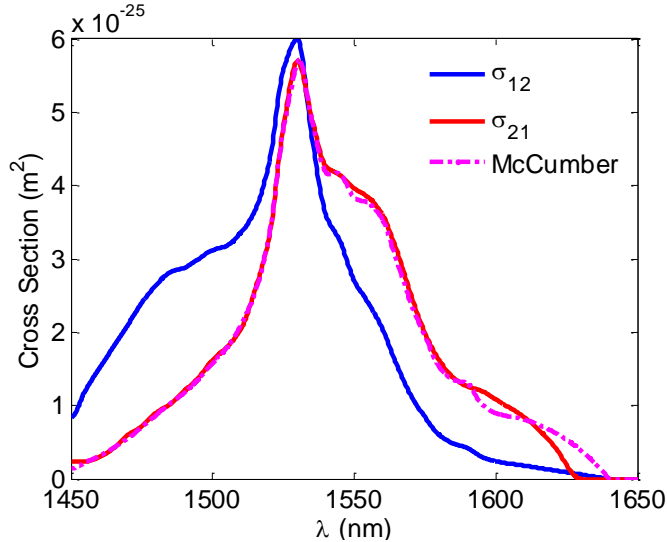


**Fig. 1:** Absorption  $\sigma_{12}$  and emission  $\sigma_{21}$  cross-sections of erbium in silica fibers.

The photon population in pumped edf at the  $1550\text{nm}$  regime results from spontaneous and stimulated emissions. Spontaneous radiation allows photon emission and absorption-reemission processes at different wavelengths in any direction, where only a small part of those emitted photons,  $\kappa \sim 0.01 - 0.02$  remains in the fiber<sup>32</sup>. In a stimulated radiation the emitted photons replicate the wavelength and the direction of the impinging photons and therefore most of them are kept in the fiber. Below inversion, the population in the second level  $N_2$  is on average lower than in the first state  $N_1$ , meaning that the spontaneous emission is important. However there are wavelengths regions with  $\sigma_{21}(\lambda) > \sigma_{12}(\lambda)$  where the stimulated emission increases. Therefore, the photon gas starts at the pump input in the fiber with spontaneous and stimulated emissions, and as the pump is depleted after a short distance, the photons propagate at highly non-inverted environment, undergoing spontaneous absorption-emission cycles that lead to thermalization and also stimulated emissions that replicate the spectrum. Therefore, it is possible to reach thermalization in an open fiber as the photons propagate along it, as shown in the experimental part, although most of the photons from spontaneous emission radiate out of the fiber and are lost.

A bosonic system in thermal equilibrium has a Bose-Einstein (BE) distribution, here the spectrum,  $p(\varepsilon) \propto g\varepsilon/[e^{\beta(\varepsilon-\mu)} - 1]$ , where  $\varepsilon = h\nu = hc/(n_r\lambda)$  is energy,  $h$  is the Planck constant,  $\beta = k_B T$ ,  $T$  is temperature,  $k_B$  - the Boltzmann constant and  $\mu$  - the chemical potential.  $g$  is the degeneracy or density of states (DOS) which is independent of  $\nu$  for a 1D photon gas with a regular linear dispersion. Usually the photon number is not conserved and  $\mu=0$ , as we have in black-body radiation. In optical cavities and lasers, the photon number is in many cases conserved by pumping that compensates for the unavoidable losses. However, for TE and BE distribution there are additional conditions. In the dye-filled microcavity experiment<sup>7,8</sup>, for example, the photon system, that had to meet certain strict conditions, was considered a grand-canonical ensemble with  $\mu \neq 0$ . In our work we find that many of those requirements are relaxed. TE is observed here in regular 1D fiber lasers, in the lasing regime with T-LWI, and even in open fibers without the need of micron-size cavities, high finesse, or a very high capture of the spontaneously emitted photons in all directions and a cutoff frequency<sup>7,8</sup>.

For the T-LWI effect we briefly explain the central idea and give below the experimental demonstration and the theoretical results using the rate equations, given in the Appendix. We emphasize again that it is not a quantum interference LWI effect, but results from the difference between the erbium emission and absorption cross sections,  $\sigma_{12}(\lambda)$  and  $\sigma_{21}(\lambda)$ , shown in Fig. 1. We can see right away from the rate equation (Eq. 2) for  $p(\nu)$  or  $n(\nu)$ , the possibility of LWI,  $N_2 < N_1$ , at wavelengths with a larger emission than absorption cross section, when

$$N_2 B_{21}(\nu) > N_1 B_{12}(\nu) . \quad (1)$$

The lower population at the upper state is simply compensated by the higher emission than absorption rate. Therefore, even without an overall inversion, the stimulated emission can be larger than the absorption and when it increases beyond the balance with the cavity losses it provides gain and lasing. Another small effect at this wavelength region is the slight deviation (seen in Fig. 1) from the McCumber relation<sup>27-29</sup>. We show below T-LWI at the high wavelength side of the thermal spectrum,  $\sim 1605\text{nm}$ , an unusual wavelength for edf fiber lasers.

We turn to the experiment and the measurements with edf ring cavities and open fibers and after that we discuss the theoretical results. We used edf with various erbium concentrations and gain figures: 30m of 11dB/m, 300m of 1dB/m and 30m and 100m of 30dB/m. It is important to emphasize right away that the results were quite similar for the four different fibers, and we show here only a few spectra. The pumping was at a 980nm wavelength except for one case that it was with amplified spontaneous emission (ASE) of edf at the 1550nm region. The ring edf cavity had regular laser losses mostly from connectors and the output coupler of 10%. It is therefore a low finesse cavity, but since it is (30-300)m long it has a relatively long photon lifetime  $t_c \sim (10^{-6} - 10^{-7})\text{s}$  and can be regarded as a low-loss cavity<sup>12,13</sup>. The mean free path  $l_p$  for successive photon-erbium interaction (emission-absorption cycle) depends on the erbium concentration  $N_d$  (which is usually of a few 100-1000 ppm,  $N_d \sim 10^{25} \text{ m}^{-3}$ ) and the wavelength, and is given by  $l_p \approx [\sigma_{12}(\lambda)N_d]^{-1} \sim (0.1 - 1)\text{m}$  that corresponds to a time scale of  $t_p \approx l_p / (c/n_r) \sim (0.5 - 5)\text{ns}$ . (In silica fibers  $n_r \approx 1.444$  at  $\lambda \sim 1550\text{nm}$ ). Therefore, thermalization that needs a few photon-erbium interaction cycles<sup>7,8</sup> can occurs within a few meters, even in open fibers, that is quite surprising. It is surely the case in our fiber cavity

systems where we have  $(t_c/t_p) \sim 20 - 2 \times 10^3$  interaction cycles, sufficient for photon thermalization at most of the relevant wavelength region. We note that in the high-finesse dye-filled microcavity the photon lifetime was much smaller (sub ns regime) because the cavity length was only  $l \approx 1.5 \mu m$ , but the mean free path there was also small. The edf cavity case can therefore fall in the low-loss category in Eqs. 3 and 4, which distinguishes the BE-BEC regime from lasers<sup>12,13,25,26</sup>, (but such low loss situation occurs in many lasers.) Nevertheless, as was already mentioned, there is another essential loss part below inversion in our fiber systems due to the low fraction  $\kappa \approx 1 - 2\%$  of the stimulated emission photons that is kept in the fiber cavity, while the rest radiates at all directions<sup>32</sup>. It means that there is a large loss factor of 98-99% at each spontaneous emission event. This loss does not stop the thermalization as we find in our experiments that are supported by the analysis and the theoretical spectra shown below. This loss factor  $\kappa$  appears in the numerator of the BE distribution (Eqs. 3 and 4) and simply reduces the overall intensity, but does not change the distribution.

Figs. 2-5 give experimental spectra with corresponding BE lines given by (Eq. 4)  $p(v) \propto \kappa g h v / (e^{\beta[hv-\mu]} - 1) = [\kappa g h c / (n_r \lambda)] (e^{\beta[hc/(n_r \lambda) - \mu]} - 1)$ . They show BE distribution (the almost straight line parts in the semi-log plots) at a broad spectral range up to 50-200nm, and with higher pumping a coexistence of BE spectra with lasing without an overall inversion at the high wavelength side, around  $\lambda \approx 1605nm$ . Figure 2 gives experimental spectra for an edf ring cavity measured at a room temperature,  $\sim 300K$ , and Fig. 3 at a liquid Nitrogen temperature,  $77K$ . They show broad thermal spectra (the straight line parts) which nicely match the BE distribution at a broad wavelength region for both temperatures. At  $300K$  for low pumping, the BE band reaches  $\sim 90nm$  and for higher pumping it spans over  $\sim 150nm$ . The lasing peaks are at the right side of the BE spectral band. At  $77K$  the logarithmic BE slope is  $300/77 \approx 3.9$  times higher than the  $300K$  slope, as the theory predicts, but the spectral range is only  $\sim 50nm$  and the lasing is slightly shifted to a lower wavelength. We don't elaborate here on the effect of the chemical potential that can be disregarded in most of the band, except for the edge, as seen in the experimental spectra. It is more important for the BEC study that we will discuss in a future paper. Figure 4 shows experimental spectra for an open  $30m$   $11dB/m$  edf, and Fig. 5 for a cavity and open  $100m$ ,  $30dB/m$  edf, both at a room temperature. In this experiment the BE spectral band reaches  $\sim 200nm$  and in the cavity case it is accompanied by a sharp oscillation line at the right

side, that is again T-LWI. Here we used a different kind of pumping directly from the first to the second level by ASE of an edf fiber with a spectrum centered around  $1550\text{nm}$ . In the laser case this pumping was inside the cavity. It is striking to see the broad BE spectral spreading out of the narrow spectrum pumping. The thermalization process spreads and transforms the photons from low to higher wavelengths. Thus, TE can be reached not only in close cavities, but also in open fibers, as the photons propagate and become thermalized. In the distributed rate equation model that we calculated but don't show here, we could see how the photon thermalization develops along the propagation in the fiber as the distance is larger than  $l_p$ .

The TE is obtained significantly below inversion, but when the pumping was increased in the cavity case, lasing started without an overall inversion at an unusually long wavelength of  $\sim 1605\text{nm}$ , as seen in Figs. 2-5. It is the high wavelength side of the broad TE band. We observed in some cases hysteresis and bistability and the lasing spectral part switched from CW to pulsation. It can be attributed to a saturable absorber mechanism of the edf similar to passive mode-locking. We also note that one has to be careful about oscillation without inversion, when attributing it to lasing, that in some cases can be BEC<sup>17</sup>. We will report on this topic in the future.

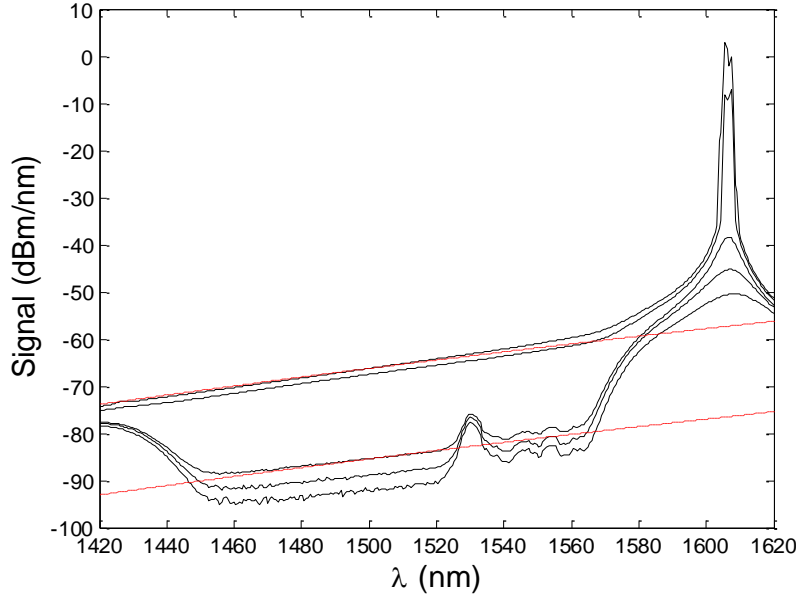


**Fig. 2:** Experimental spectra for a fiber cavity at a room temperature ( $\sim 300\text{K}$ ). The measured spectra (black lines) correspond to pumping of 44.67, 51.2, 53.58, 53.83, and 208.0 mW. The measurements shown here were taken from a ring fiber cavity consisting of 30m of 11dB/m polarization maintaining edf. The dashed red lines are the theoretical thermal BE distribution for 300K. The BE spectral bands (the almost straight line parts in the semi-log plots) for low pumping are at (1450-1530)nm and for higher pumping at (1420-1570)nm. For strong pumping we can see at the right side of the BE spectra (staright lines) a strong lasing line, that in certain conditions can be associated with BEC.

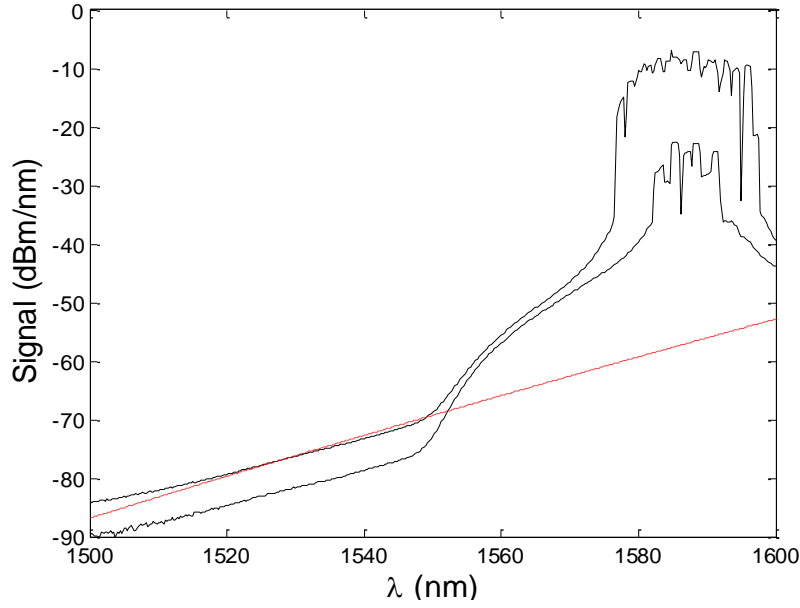


**Fig. 3:** Experimental spectra in an edf fiber cavity at 77K. The measured spectra correspond to pumping levels of 12 and 162 mW. The measurements shown here were taken from a ring fiber cavity consisting of 30m of 11dB/m polarization maintaining edf. The BE bands (the straight line pzsrt). The dashed red line is the theoretical thermal BE distribution for 77K. The BE band is at (1500-1550)nm. For strong pumping we can see at the right side of the BE spectra strong lasing lines.

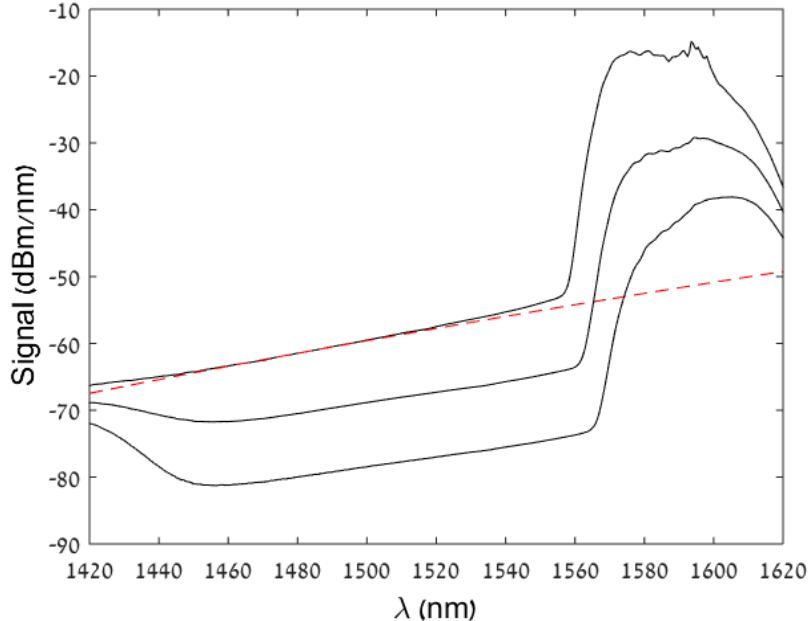


**Fig. 4:** Experimental spectra in an open fiber at a room temperature. It was obtained with 30m of 11dB/m edf. The measured (black) lines correspond to 67.6, 88.6, and 153.6mW pumping. The open fiber is. Dashed red line – TE slope for 300K. The BE band (the straight line parts) reaches ~115nm.

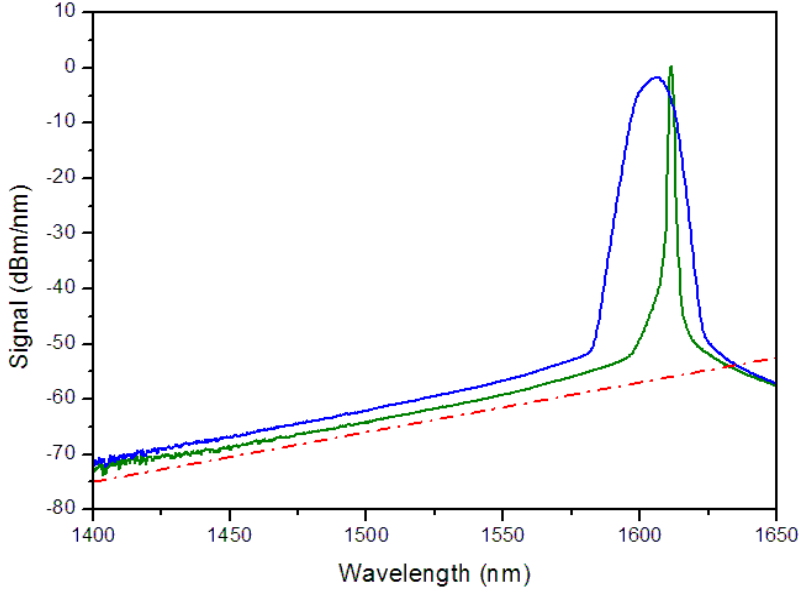


**Fig. 5:** Experimental spectra from an open fiber (blue line) and a cavity (green) at a room temperature. It was obtained with a 100m, 30dB/m edf. The BE spectral band (almost straight lines) spans over  $\sim 200\text{nm}$ , besides a sharp oscillation line (T-LWI) for the cavity case at the right side. The dashed red line shows the BE slope at 300K without including the chemical potential correction that affects the right side of the spectrum. The pumping here was with ASE of edf while the pumping in all other experiments was with the usual 980nm wavelength.

The theoretical analysis is based on the lumped or the distributed rate equations models, described in the Appendix. Figure 6 shows broad BE spectra ( $>120\text{nm}$ ) calculated by the lumped model for a low cavity loss. The results are in a good agreement with the experiment, showing a large band ( $>120\text{nm}$ ) of thermal spectrum. These figures also show T-LWI with typical values of  $N_2/N_d \sim 0.18$ , that is much below inversion. The distributed model is solved numerically and gives as well similar spectra and a very good match to the experimental measurements.

The drastic difference between the thermal and regular lasers spectra is seen by comparing Figs. 6 and 7. The thermal lasers with broad BE spectra have low cavity losses. We used in Fig. 6 typical photon lifetime of  $t_c = 10^{-6}\text{s}$  that fits our fiber lasers, and also for zero loss ( $t_c \rightarrow \infty$ ). This broad BE spectra is very different from Figure 7, the spectra of a regular laser with a higher cavity loss and  $t_c = 2.3 \times 10^{-9}\text{s}$ . It is in accordance with the theoretical study that differentiates TE and BEC from lasers by losses<sup>12,13,25,26</sup>, except that the spontaneous emission loss is very high in our systems. Remarkably, the very simple lumped model fits our experiments, the dye microcavity<sup>7,8</sup>, regular lasers and photon-BEC behavior.

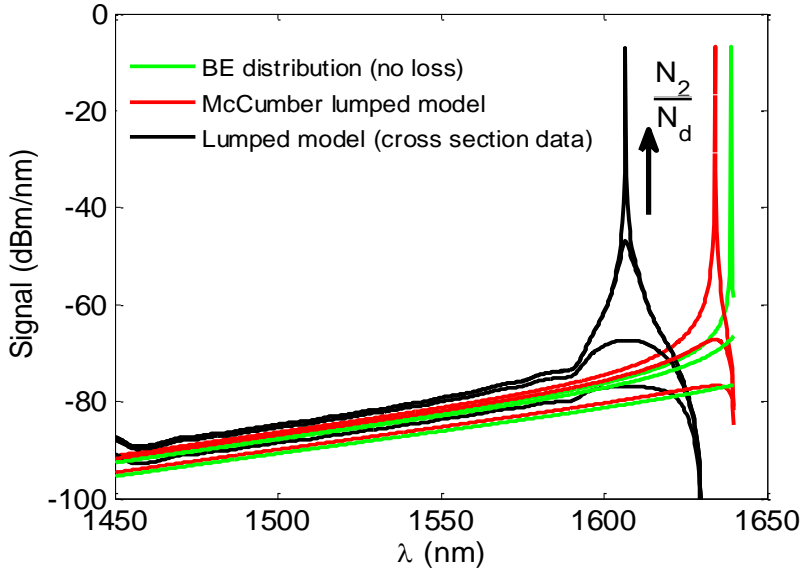


**Fig. 6:** Theoretical spectra of a fiber cavity at 300K with a broad BE regime (the straight lines in the semi-log plots), calculated by the lumped rate equation model (Eq. 2) for a low-loss cavity with photon lifetime  $t_c = 10^{-6} s$ . The black lines correspond to solutions of the rate equation for increasing values of the population ratio until the threshold value:  $N_2 / N_d = 0.09, 0.162, 0.179, 0.18$ . The figure also shows spectra calculated from the rate equation with a cross section enforced by the McCumber relation. The red lines are for  $t_c = 10^{-6} s$  and the green lines for  $t_c \rightarrow \infty$  (no cavity loss), with the above inversion and a slightly different threshold value, showing oscillation (BEC?) at the band edge.

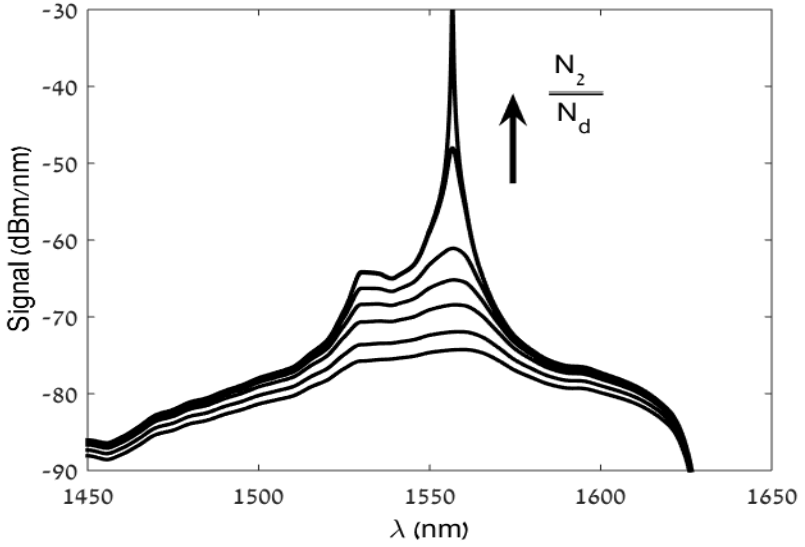


**Fig. 7:** Theoretical spectra for a regular edf laser oscillation calculated by the lumped rate equation model (Eq. 2) for 300K. It is the relatively high cavity loss regime with  $t_c = 2.3 \times 10^{-9} s$ . The spectrum here is very different from the low loss thermal BE regime and the lasing is at 1656.6nm. The lines correspond to increasing values of the population ratio until their threshold value:  $N_2 / N_d = 0.31, 0.372, 0.434, 0.496, 0.558, 0.6193, 0.62$ .

Fig. 8 shows the upper level population population ratio  $N_2/N_d$  as the photons propagate in the fiber, obtained from the distributed model (Eq. 5). This model includes an equation for the pump that implies its depletion after a short distance in the edf. It shows that the upper state population quickly falls to a small value. In the case with the oscillation, the population ratio stabilizes at a finite value well below inversion ( $\sim 0.18$  for the experiment parameters), showing the T-LWI phenomenon.

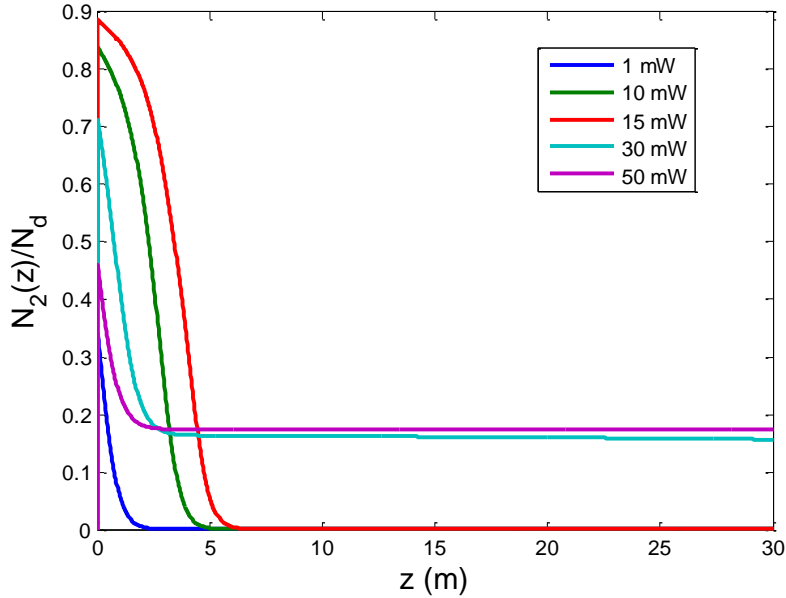


**Fig. 8:** Theoretical upper state population fraction  $N_2(z)/N_d$  along an edf fiber for various pumping levels. Calculated by the distributed rate equations model (Eq. 5). Below lasing (blue, green and red curves)  $N_2/N_d$  drops down to near zero values after a short propagation in the fiber. Above the lasing threshold (purple and sky blue curves) the upper state population fraction is almost constant along the fiber and approaches an average value of 0.18 that is much below inversion, showing the T-LWI phenomena.

We finally add a few notes. First that for most lasers that are narrow-band it is still correct to say that they are not in TE and that the condition for their lasing is population inversion. Nevertheless, TE and T-LWI can be expected in other broadband lasers and there can be other mechanisms, beyond the thermal one, for spectral broadening that can yield LWI. We also add that such lasers can open a way for a special possibility of channeling broad spectral light into a single frequency lasing or Bose-Einstein condensation (BEC) at the high wavelength edge of the thermal spectrum. We note on the possibility to observe BEC in edf cavities. An important step for it is thermalization of the photon gas that is obtained in the present work.

There are a few other soluble issues, such as a requirement on the density of states in 1D cavities, reaching the critical power for BEC that we estimate to be in the  $\mu W - mW$  region, and the need of a frequency cutoff to set a reference frequency, the ground-state, for the condensation. We already were able to obtain photon-BEC in the theoretical analysis and expect to observe it experimentally in fiber cavities at a room temperature.

## Appendix:

We elaborate here on the theoretical base of the lumped and distributed rate equations. The lumped model gives the basic results shown in the theoretical figures that nicely describe the experimental spectra. The second distributed rate equations model allows following the pump and signal propagation along the fiber (z-dependence).

### 1. The lumped rate equation model:

We first describe a lumped model that gives the basic results. As in the dye microcavity system<sup>25,26</sup>, the photon population and its dependence on frequency is governed by a rate equation where the erbium atoms are modeled as broadened two level systems:

$$\frac{dn(\nu)}{dt} = \kappa N_2 A(\nu) + N_2 B_{21}(\nu) n(\nu) - N_1 B_{12}(\nu) n(\nu) - n(\nu) / t_c \quad (2)$$

The Einstein A-B relation here takes the form  $A(\nu) = B_{21}(\nu)g(\nu)$ , with  $g(\nu)$  as the mode degeneracy or DOS (constant in 1D with a linear dispersion). The steady state solution of the rate equation is

$$n(\nu) = \frac{\kappa g(\nu)}{\frac{t_c^{-1} + N_1 B_{12}(\nu)}{N_2 B_{21}(\nu)} - 1} \quad (3)$$

For  $t_c^{-1} \ll N_1 B_{12}(\nu)$  with the McCumber<sup>25,26,27</sup> (or Kennard-Stepanov<sup>28,29</sup>) relation

$B_{12}(\nu) / B_{21}(\nu) = \sigma_{12}(\nu) / \sigma_{21}(\nu) = C e^{\beta h\nu}$  where C is constant, Eq. 2 reduces to the BE distribution and spectrum:

$$\begin{aligned} n(\nu) &= \kappa g(\nu) / (e^{\beta(h\nu - \mu)} - 1) \\ p(\nu) &\propto n(\nu)h\nu = \kappa g(\nu)h\nu / (e^{\beta(h\nu - \mu)} - 1). \end{aligned} \quad (4)$$

The chemical potential is defied by  $e^{\beta\mu} = C N_1 / N_2$ ,  $\sigma_{ij}(\nu) \propto B_{ij}(\nu)$  are the absorption and emission cross sections  $\sigma_{12}(\lambda)$  and  $\sigma_{21}(\lambda)$  related to transitions between the first and second levels (shown in Fig. 1), and  $B_{ij}(\omega)$  are the Einstein coefficients.

## 2. The distributed rate equation model:

The theoretical base for T-LWI in our system is derived from an extension of the above model to distributed (z-dependence) rate equations for the populations, where the erbium atoms are modeled as broadened two level systems. It gives more insight on the dynamics inside the cavity and includes information about the propagation of the signal and the pump along the fiber  $z$ -axis. The model consists of the following set of coupled equations (in the two-level approximation) for the pump power  $P(z)$ , signal power  $p(\nu, z) \propto n(\nu, z)h\nu$ , and the population densities  $N_1(z)$  and  $N_2(z)$ , where  $n(\nu, z)$  is the photon population density,  $N_1(z) + N_2(z) = N_d$  is the erbium atom density, and we also give typical numerical values for the parameters):

$$\begin{aligned} \frac{dP(z)}{dz} &= -\sigma_p N_1(z) \\ \frac{dp(\nu, z)}{dz} &= [\sigma_{21}(\nu)N_2(z) - \sigma_{12}(\nu)N_1(z)]p(\nu, z) + \kappa N_2(z)\sigma_{21}(\nu)g(\nu)h\nu \\ \frac{dN_2(z)}{dt} &= \sigma_p N_1(z) \frac{P(z)}{h\nu_p A_p} + \int d\nu \sigma_{12}(\nu)N_1(z) \frac{p(\nu, z)}{h\nu A_s} - \int d\nu \sigma_{21}(\nu)N_2(z) \frac{p(\nu, z)}{h\nu A_s} - \frac{N_2}{t_{sp}} = 0 \end{aligned} \quad (5)$$

The first equation describes the pump  $P(z)$  absorption by the ground level atoms with a cross section  $\sigma_p \approx 2.6 \cdot 10^{-25} m^2$ . The starting condition is set by  $P(z=0) = P_0$ . The second equation describes the propagation of the signal spectrum  $p(\nu, z)$ , governed by stimulated absorption and emission, and on a fraction  $\kappa$  of the spontaneous emission. The starting condition for this equation depends on the fiber geometry:  $p(\nu, 0) = p_{in}(\nu)$  for open fibers, and  $p(\nu, 0) = R p(\nu, L)$  for close cavities, where  $R$  is the output coupler reflection. The third equation describes the population dynamics of  $N_{1,2}(z)$ . Here,  $A_p$ ,  $A_s$  are the pump/mode overlap areas with the fiber core ( $A_p, A_s \sim 24 \mu m^2$ ), and  $t_{sp} \approx 10^{-2} s$  is the spontaneous emission time.

## **References:**

1. A. Javan, *Phys. Rev.* **107**, 1579 (1957).
2. S. E. Harris, *Phys. Rev. Lett.* **62**, 1033–1036 (1989).
3. M. O. Scully, Y. S. Zhu, A. Gavridiles, *Phys. Rev. Lett.* **62**, 1813 (1989).
4. M. O. Scully, M. Fleischhauer, [\*Science\* 263, 337 \(1994\)](#).
5. A. S. Zibrov, M. D. Lukin, D. E. Nikonov, L. W. Hollberg, M. O. Scully, V. L. Velichansky, H. G. Robinson, *Phys. Rev. Lett.* **75**, 1499 (1995).
6. K. J. Boller, A. Imamoglu, S. E. Harris, *Phys. Rev. Lett.* **66**, 2593 (1991).
7. J. Klaers, J. Schmitt, F. Vewinger, *Nature* **468**, 545 (2010).
8. J. Klaers, F. Vewinger, M. Weitz, *Nat. Phys.* **6**, 512-515 (2010).
9. R. Balili, V. Hartwell, D. Snoke, L. Pfeiffer, K. West, *Science* **316**, 1007 (2007).
10. H. Deng, G. Weihs, C. Santori, J. Bloch, Y. Yamamoto, *Science*, **298**, 199 (2002).
11. S. O. Demokritov, V. E. Demidov, O. Dzyapko, G. A. Melkov, A. A. Segre, B. Hillerbrands, A. N. Slavin, *Nature*, **443**, 430 (2006).
12. P. Kirton, J. Keeling, *Phys. Rev. Lett.* **111**, 100404 (2013).
13. P. Kirton, J. Keeling, *Phys. Rev. A*, **91**, 0332826 (2015).
14. A. Chiocchetta, I. Carusotto, *Phys. Rev. A*, **90**, 023633 (2014).
15. D. Bajoni, P. Senellart, A. Lemaitre, J. Bloch, *Phys. Rev. B* **76**, 201305(R) (2007).
16. A. Rückriegel, P. Kopietz, *Phys. Rev. Lett.* **115**, 157203 (2015).
17. B. Fischer, R. Weill, *Opt. Express* **20**, 26704 (2012).
18. R. Weill, B. Levit, B. Bekker, O. Gat, B. Fischer, *Opt. Express* **18**, 16520 (2010).
19. R. Weill, B. Fischer, O. Gat, *Phys. Rev. Lett.* **104**, 173901 (2010).
20. G. Oren, B. Bekker, B. Fischer, *Optica* **1**, 145 (2014).
21. M. Zhurahov, A. Bekker, B. Levit, R. Weill, B. Fischer, *Opt. Express* **24**, 6553 (2016).
22. C. Sun, S. Jia, C. Barsi, S. Rica, A. Picozzi, J. W. Fleischer, *Nat. Phys.* **8**, 470 (2012).
23. C. Connaughton, C. Josserand, A. Picozzi, Y. Pomeau, S. Rica, *Phys. Rev. Lett.* **95**, 263901 (2005).
24. C. Conti, M. Leonetti, A. Fratalocchi, L. Angelani, G. Ruocco, *Phys. Rev. Lett.* **101**, 143901, (2008).
25. J. Klaers, J. Schmitt, T. Damm, F. Vewinger, M. Weitz, *Appl. Phys. B*, **105**, 17 (2011).
26. J. Schmitt, T. Damm, V. Dung, F. Vewinger, J. Klaers, M. Weitz, *Phys. Rev. A* **92**, 011602 (2015).
27. E. Desurvire, *Erbium-doped fiber amplifiers*, (John Wiley Publication, 1994).
28. D. E. McCumber, *Phys. Rev.* **134**, 299 (1964).

29. R. M. Martin, R. S. Quimby, *J. Opt. Soc. Am. B*, **23**, 1770 (2006).
30. E. H. Kennard, *Phys. Rev.* **28**, 672 (1926).
31. B. I. Stepanov, *Dokl. Akad. Nauk SSR* **112**, 839 (1957).
32. T. Sondergaard, B. Tromborg, *Phys. Rev. A*, **64** *Phys. Rev. A* **64**, 033812 (2001).

**Acknowledgments:** This research was supported by the Israel Science Foundation (ISF) and the Pazy Foundation.